Materialia 13 (2020) 100857

Contents lists available at ScienceDirect

Materialia

journal homepage: www.elsevier.com/locate/mtla

Full Length Article

Confirmation of rapid-heating β recrystallization in wire-arc additively manufactured Ti-6Al-4V

A.E. Davis[a,*], A. Caballero[b], P.B. Prangnell[a]

[a] Department of Materials, University of Manchester, Manchester M13 9PL, United Kingdom
[b] Welding Engineering and Laser Processing Centre, Cranfield University, Bedfordshire MK43 0AL, United Kingdom

ARTICLE INFO

Keywords:
Titanium
Grain refining
Plastic deformation
Recrystallization texture
Electron backscattering diffraction (EBSD)

ABSTRACT

The coarse columnar β grains in Ti-6Al-4V WAAM can be refined by relatively low strain inter-pass deformation. Simulation, with rapid heating, has shown this may partly occur by a novel recrystallization mechanism that involves twinning during β regrowth through the α-β transus, as a result of the prior deformation promoting faults in the α-β interface, which produces a unique micro-texture in each parent β grain. Here, this potential mechanism has been investigated further, using a different deformation mode – uniaxial tensile deformation rather than plane strain compression – to enable the texture contribution from conventional recrystallization to be more unambiguously discriminated. The tensile-deformed samples are shown to produce the same unusual unique micro-texture seen previously, at low strains, despite the different deformation mode, but this disappeared at higher strains, which provides more evidence in support of this new rapid heating β recrystallization mechanism.

1. Introduction

Direct energy deposition additive manufacturing (AM) processes, like wire-arc AM (WAAM) with titanium alloys such as Ti-6Al-4V (Ti64), have been the focus of recent research due to their high deposition rate and ability to produce near-net-shape components with size envelopes of several metres [1–8]. However, in Ti64 WAAM under standard conditions, epitaxial growth during solidification typically produces cm-long columnar β grains, with a $<001>_\beta$ fibre texture, which can sometimes extend throughout the entire build height [6,9–14]. This arises because the heated melt pool promotes a steep thermal gradient at the solidification front and Al and V have partition coefficients close to unity, which together produce minimal constitutional undercooling and a narrow mushy zone, inhibiting nucleation ahead of the solidification front [15–19].

It has been shown that inter-pass deformation with a modest plastic strain is surprisingly effective at breaking up the coarse β-grain structures and reducing the β texture produced in the WAAM process. Martina et al. have demonstrated that layer-height compression by as little as 8% [9,10], using rolling, is only required to refine the β-grain structure by 'recrystallization' on re-heating through the β transus. Using plane strain compression (PSC) and rapid-heating simulations, the current authors have suggested [12,20] that this behaviour may partly stem from a novel recrystallization mechanism (*rapid-heating β RX*) that is unique to the specific AM conditions. An example of this mechanism is shown in Fig. 1a where a matchstick sample deformed in plane strain by ~14% was rapidly heated above the β transus, while the grip-cooled ends were kept below. This allowed direct comparison of the parent β and recrystallized grains in the same sample, demonstrating that this recrystallization mechanism produces a unique, four-fold motif micro-texture in each parent β grain (an ideal example of this is given in Fig. 1b). Modelling of the potential β twinning relationships [20] has indicated that a double {112}<111> twinning of β can create these new grain orientations during rapid heating of a fine, lightly deformed, lamellar microstructure. It has been postulated that this may occur because, in the fine lamellar microstructure produced by rapid cooling in the WAAM deposits, the migrating α-β interfaces encounter dislocations, causing growth faults that nucleate annealing twins [21] when the β phase regrows during the $\alpha \rightarrow \beta$ transformation. A schematic of this proposed mechanism has been reproduced from [12] in Fig. 1c. To date, rapid-heating β RX has only been studied in simulations of the current inter-pass deformed WAAM processes, conducted using PSC tests [10,12,20]. However, when larger strains were employed in these tests (> 20%), after rapid β annealing and recrystallization, new single texture components emerged in these samples whereby the $<001>_\beta$ // ND component was rotated ~ 30° about the constraint and expansion axes. These new components originated from bands of recrystallized grains formed in intense macro-shear bands that developed in the samples at higher compression ratios, which overlapped with the distinctive four-fold motif texture associated with the rapid-heating β RX texture [12].

* Corresponding author.
E-mail address: alec.davis@manchester.ac.uk (A.E. Davis).

https://doi.org/10.1016/j.mtla.2020.100857
Received 22 June 2020; Accepted 31 July 2020
Available online 13 August 2020

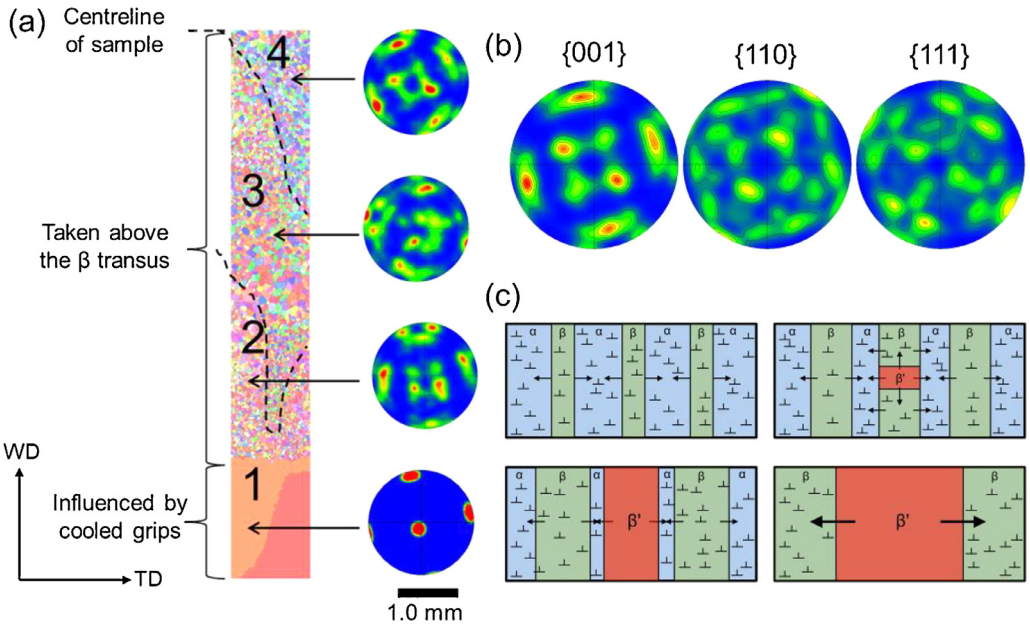

Fig. 1. (a) An example simulation of the inter-pass deformation WAAM process, where a lightly deformed (ε = ~14%) matchstick sample was rapidly heated above the β transus, while the grip-cooled sample end remained below. The $\{001\}_{\beta}$ pole figures show the orientations of the original parent β grain, 1 (not heated above the β transus), and recrystallized grain regions 2–4, corresponding to the prior parent grains. Grain 1 is the parent to the recrystallized grain in region 2, allowing a direct comparison of the 'before and after' texture. Figure adapted from [20]. It can be noted that the same unique micro texture is seen in each recrystallized parent grain as depicted in (b), which shows the idealised rapid-heating β RX four-fold texture component, also adapted from [20]. (c) The proposed rapid-heating β RX mechanism where the migrating α-β boundary in a deformed $\alpha + \beta$ microstructure causes a stacking fault to occur which grows into a twin. The strain-free nucleated twin (β') gains a growth advantage over the surrounding β and consumes it, resulting in a 'recrystallized' grain. Figure reproduced from [12].

Table 1
WAAM build parameters.

Heat Source Parameters		Gas Flow Rates	
Wire feed speed	37 mm s^{-1}	Plasma gas flow rate	1 l min^{-1}
Travel speed	5.5 mm s^{-1}	Shielding gas flow rate	15 l min^{-1}
Current	160 A		

The new components were related to rotation of the parent orientation within the shear bands, which were formed by the tool-sample friction conditions in the PSC tests that created new β orientations in the deformation microstructure, and called into question whether the proposed concept of an annealing-twin RX mechanism was indeed correct.

Therefore, in this work, to confirm whether the rapid-heating β RX mechanism that produces the unusual micro-texture depicted in Fig. 1b is a consequence of local shear specific to the PSC deformation conditions, or is a result of β annealing twinning [22–25], a WAAM sample with a columnar β-grain structure was deformed under a completely different mode - in uniaxial tension. The logic behind this approach to further test the concept of a twinning-based recrystallization mechanism is that, in the case of conventional recrystallization, the micro-texture will be related to orientations already present in the deformed sample, so that this change of deformation mode should produce a different texture on recrystallization to PSC. In addition, deformation in a tensile sample will be free of PSC tool-friction-related strain-localisation shear band effects.

2. Materials and methods

To perform this experiment, dog-bone tensile specimens were machined from a WAAM wall, parallel to the build direction and columnar β-grain structure. The sample was built using a 1.2 mm diameter Ti64 wire with the process parameters provided in Table 1. The WAAM process is described fully in ref. [5]. The reference frame employed is defined as: heat-source travel, or wall, direction ≡ WD, transverse direction ≡ TD, and the build-height, or layer normal direction ≡ ND. Tensile specimens with a gauge length (// ND), width (// TD), and thickness (// WD) of 29, 6.4, and 6.4 mm, respectively, were deformed at a speed of 0.01 mm s^{-1} until failure occurred. Two samples were then cut from each specimen: a section from the grips and the necked region to a distance of ~ 14 mm from the fracture surface, which, after applying a rapid heat treatment to the latter, were ground down to the sample centre length-width (ND-WD) plane. The latter deformed sample was rapidly heated in a TA Instruments DIL 805A/D/T quench-dilatometer, at a rate of ~ 500 °C s^{-1} (representative of the WAAM process [11]) above the β transus to ~ 1100 °C and held for 5 s to ensure complete transformation to β. The samples were then metallographically prepared for scanning electron microscopy (SEM) by polishing to an OPS finish.

Electron backscatter diffraction (EBSD) orientation maps were collected using a voltage of 20 kV and a current of 16 nA, in a Tescan Mira3 FEG-SEM, equipped with an Oxford Instruments' Symmetry EBSD detector and AZtec acquisition software. β-phase orientation maps were reconstructed from the α phase using software developed by Davies and Wynne (for full details see refs. [26–29]). EBSD data was processed using HKL Channel5 software, and EBSD maps are displayed throughout in inverse pole figure (IPF) colouring, with respect to ND, with high (> 15°) and low (< 15°, > 5°) angle grain boundaries (HAGBs and LAGBs) highlighted in black and white, respectively. LAGBs were set to be above 5° to avoid highlighting artefacts of the β reconstruction which were present below this misorientation. Textures are presented as contoured pole figures in multiples of random density (MRD). β-grain sizes were measured from the β-reconstructed EBSD data using HKL Channel5. The local tensile strain across the deformed necked region was estimated by measuring the sample area from metallographic sections.

3. Results and discussion

The original coarse-columnar, primary, β-grain structure, taken from the (un-heated) WAAM tensile specimen grip region, is shown is Fig. 2.

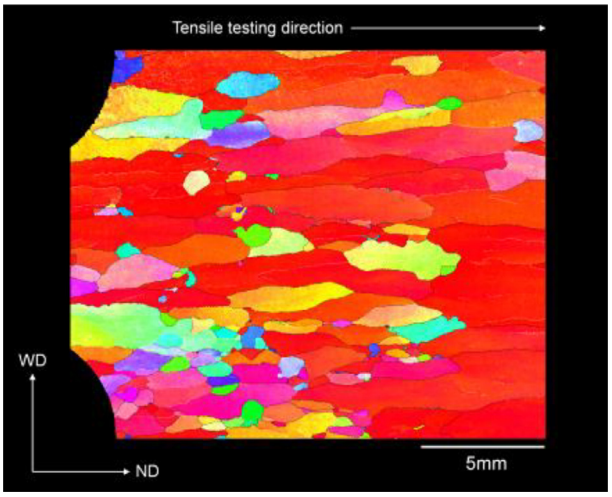

Fig. 2. β-reconstructed EBSD orientation map of the tensile specimen grip showing the typical WAAM undeformed coarse-columnar, primary, β-grain structure.

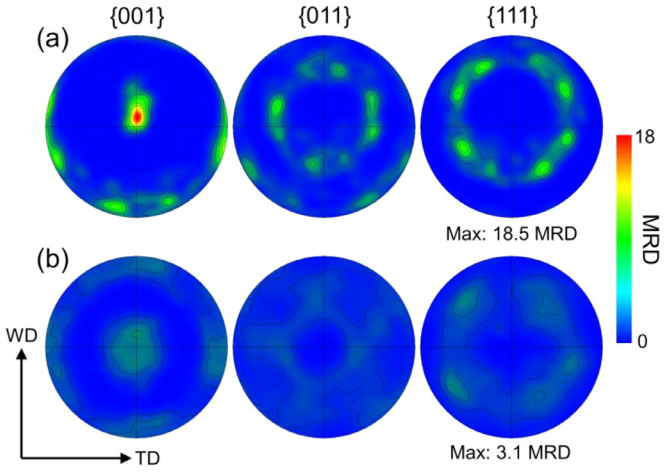

Fig. 3. 'Before and after' pole figures showing the bulk textures of the WAAM tensile specimen (a) grip (coarse columnar β structure, Fig. 2), and (b) the whole recrystallized region, following rapid re-heating, near the fracture surface (Fig. 4).

In this reconstructed β-phase EBSD orientation map, the majority of the β-grains can be seen to grow parallel to ND with a strong ND // $<001>_\beta$ fibre texture (red in IPF colouring), which is consistent with previous work [10,12,30]. The associated texture is provided in Fig. 3a and shows strong $<001>_\beta$ // ND alignment with a slight tilt towards WD, the heat source travel direction. This same grain structure, present in the whole tensile specimen gauge region, was then deformed under tension until fracture, and rapidly heated above the β transus, before being subsequently mapped using EBSD. The region analysed through the neck and down the gauge length, was particularly insightful in this regard, as it provided a tensile strain gradient in a single sample, from ~ 1 – 43%. The reconstructed-β microstructure from this region, following β annealing, is shown in Fig. 4, where a recrystallized, equiaxed, grain structure of ~ 50 μm average size can be seen on the left near the fracture surface, which coarsens slowly in size with decreasing strain and increasing distance to the right, down the gauge length, and then transitions into the parent columnar β-grain structure, as seen in Fig. 2. From the colour changes across the map from left to right, it can also be seen that there is a change in preferred orientation of the recrystallized grains from: i) the original $<001>_\beta$ // ND alignment (red) with spreading towards $<011>_\beta$ // ND (green) near the fracture surface, where there was a high strain, to ii) a bigger spread of orientations with more $<111>_\beta$ // ND alignment (blue) and much less original $<001>_\beta$ // ND alignment (red) at lower strains, before returning to (iii) the unrecrystallized region with the original as-built $<001>_\beta$ // ND alignment (red). In Fig. 3, the bulk β texture taken from the whole 100% recrystallized region is compared to the as-deposited texture and can be seen to be markedly weaker than the solidification texture, with the peak near $<001>_\beta$ // ND intensity falling to less than 3 MRD and demonstrating a spreading of ~ 30° away from the $<001>_\beta$ // ND pole in the $\{001\}_\beta$ pole figure.

When the micro-textures in the EBSD map in Fig. 4 were analysed locally along the gauge length in Fig. 4a-d, farthest away from the fracture surface where the tensile strain was below ~ 10%, the unrecrystallized large columnar grains still exhibited the as-built strong $<001>_\beta$ // ND texture (Fig. 4a). However, the pole figures from the lower strain (14 - 30%) recrystallized region in the middle of the map in Fig. 4b-c, again demonstrated an unusual mircro-texture, which can be seen to consist of a four-fold symmetrical intensity motif, centred on the original parent-grain $<001>_\beta$ poles in the $\{001\}_\beta$ pole figure, from which it is tilted away by ~ 20 - 30. Despite using an entirely different deformation mode to the PSC samples investigated previously, this micro-texture bares a strong similarity to the idealised rapid-heating β RX texture motif reported previously [12,20] and reproduced in Fig. 1b. The texture in Fig. 4c is more diffuse because it was obtained from multiple parent $<001>_\beta$ // ND orientated β grains, rather than a single parent β-grain orientation, as used in our previous simulations [12,20]. This result therefore provides further evidence for the proposal that the grain refinement found in lightly deformed WAAM materials is caused by an annealing-twin-based, rapid-heating, β RX mechanism, as this unique micro-texture has been seen again in the tensile sample and formed independently of the deformation mode; i.e. if the new β orientations were produced simply by a lattice rotation caused by deformation, they would be expected to be present within the orientation spread in the as-deformed sample, and the texture generated by uniaxial tension would be considerably different to that seen in plane strain compression, so that it is unlikely that this could produce an identical recrystallization micro-texture. The other interesting feature of this micro-texture is it fully replaces the original strong parent $<001>_\beta$ // ND intensity in the pole figure.

In addition, where the sample had deformed to a higher strain closer to the fracture surface, the micro-texture was found to change (e.g. at ~ 37% strain in Fig. 4d). In the higher strain region (above ~ 30%), the position of strongest intensity was found to have shifted back to the location of the original strong parent $<001>_\beta$ // ND pole, and the spreading of the distribution around this pole was also more axisymmetric. Given that the micro-texture changed along the tensile sample within different strain ranges, this suggests that two separate recrystallization mechanisms were dominant, in competition, depending on the prior strain level before β annealing. The appearance of other texture components at higher strains has been reported previously during PSC simulations of the WAAM inter-pass rolling process [12], where they were seen to form as a consequence of strong macroscopic shear bands developing in the PSC samples, which occurred due to the tool friction and sample geometry effects. Here, the effect of increasing strain during tensile deformation to levels above ~ 30% similarly seems to have reduced the significance of the rapid-heating β RX mechanism, but in this case – because of the different deformation mode – this has been replaced by a more symmetrical spreading of the strong parent $<001>_\beta$ // ND intensity away from the starting orientation (as seen in Fig. 4d). This change in behaviour with increasing strain is still consistent with the rapid-heating β RX mechanism proposed, which dominates at lower strains. This is because it is dependant on the migration of the α-β interfaces, where interaction with lattice defects, and defects created in the α-β interface, causes stacking faults to occur resulting in twin formation during β regrowth. In contrast, recrystallization from a nucleus already present in the deformed state requires there to have been sufficient prior deformation to generate a high enough local lattice

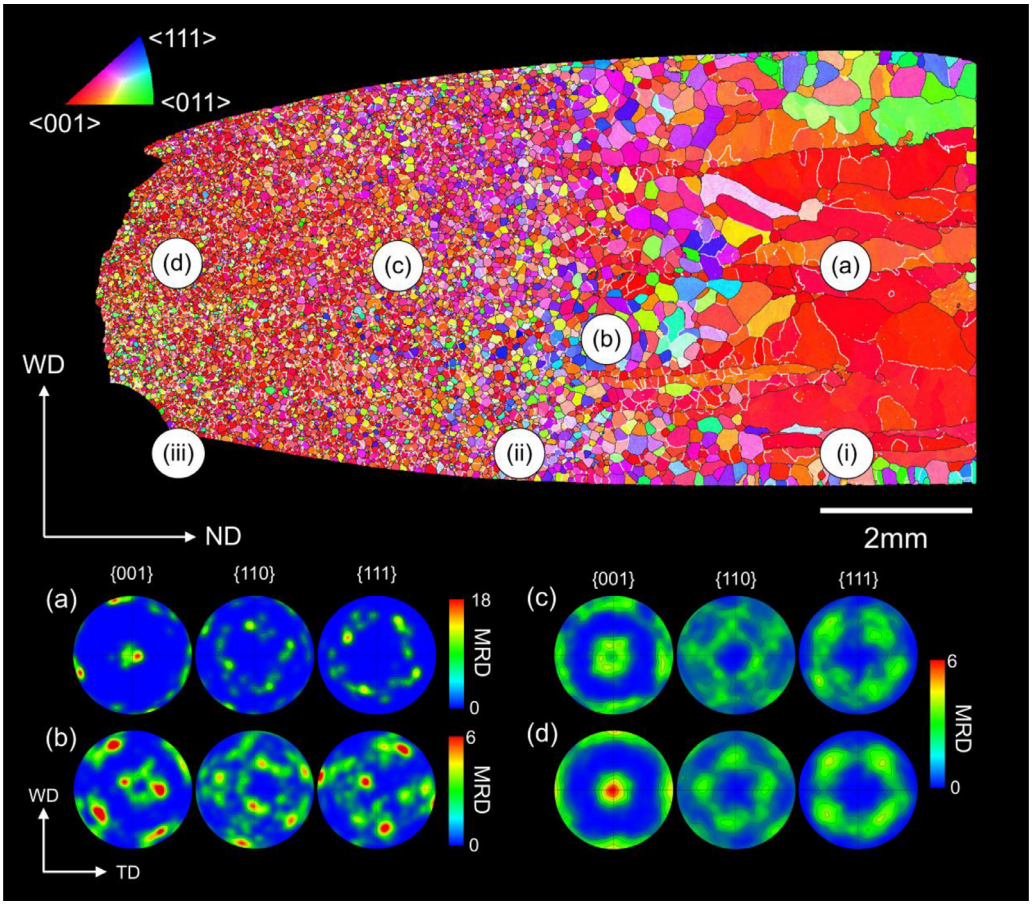

Fig. 4. β-reconstructed EBSD orientation map of the recrystallized microstructure at the centre plane of the deformed and rapidly heated sample, sectioned back from the WAAM tensile specimen fracture surface. The pole figures (a-d) show the micro-textures at the positions marked on the tensile specimen with corresponding strains of ~ 1, 15, 26, and 37%, respectively.

misorientation for a β region to acquire a more mobile grain boundary. This typically occurs in regions of plastic heterogeneity, as was observed in the macro-shear bands seen in the PSC samples studied previously [12], or at prior β–grain boundaries, or α colony boundaries, where there is greater plastic incompatibility. Increasing the strain will also lead to a general breakdown of coherency between the residual β and α, which will tend to inhibit the rapid-heating β RX mechanism. In addition, there will be a general increase in stored energy with higher strain levels, which may favour more conventional recrystallization. Although this requires further investigation, the results are consistent with two competing recrystallization processes that change in dominance as the strain level increases; from a twining-based mechanism that is unique to a fine AM microstructure with rapid heating, to a more conventional process that relies on pre-existing regions with sufficient lattice rotation to generate new β-grain nuclei.

The transition between the two different micro-textures in the tensile-deformed sample, seen as the strain increases towards the fracture surface, has been explored further in Fig. 5a. To further clarify this effect, the intensity at the parent $<001>_{\beta}$ // ND pole position has been plotted against strain in Fig. 5a. Since in our previous work using single parent grain orientations [12], it was shown that the rapid-heating β RX mechanism produces a discontinuous rotation away from the parent $<001>_{\beta}$ // ND poles (e.g. Fig. 4a) and entirely eliminates the starting orientation, the strength of the $<001>_{\beta}$ // ND pole can be used to track the contribution of the RX mechanism throughout the sample. In Fig. 5a, it can be seen that when the strain increases to ~ 10%, and recrystallization initiates, there is a very rapid drop in the $<001>_{\beta}$ // ND pole strength. As the strain increases further, the parent $<001>_{\beta}$ // ND texture then slowly re-emerges and becomes the strongest orientation for strains above 30%. In the same graph (Fig. 5a), the relative frequency of LAGBs (< 15%) has also been plotted against local strain within the gauge section, to demonstrate the concurrent change in grain-boundary character. This plot shows that, counterintuitively, there is a lower frequency of LAGBs in the low strain region of the sample (9 – 30%); i.e. the recrystallization processes operating at *lower strains* produced *more* highly misorientated grains [10,12,20]. However, as the strain level increases, the LAGB frequency starts to increase, presumably as the low strain recrystallization mechanism diminishes, but as the strain increases beyond 30% to higher strains, the LAGB frequency then begins to drop again. Together, the behaviour of these two sets of measurements are, therefore, consistent with the previously proposed annealing-twinning-based rapid-heating β RX mechanism dominating at low strains, but becoming suppressed at higher strains to be replaced by a transition to a competing more conventional recrystallization mechanism - based on new grains forming by growth from nuclei that developed by local lattice rotation in the deformed state [21,31].

Finally, the previous work that used PSC and rapid-heating simulations reported a strong near-step-function relationship between increasing strain level and the recrystallized β-grain size found in the PSC samples [12]. This plot is reproduced here in Fig. 5b and shows that rapid-heating β RX became activated at a minimum strain of 9%, but the grain size then quickly decreased rapidly to reach a minimum at 14%, past which little further refinement was observed. The grain size data from the tensile-strained sample obtained in this work has been compared to the results from the PSC simulations in Fig. 5b, using the local true

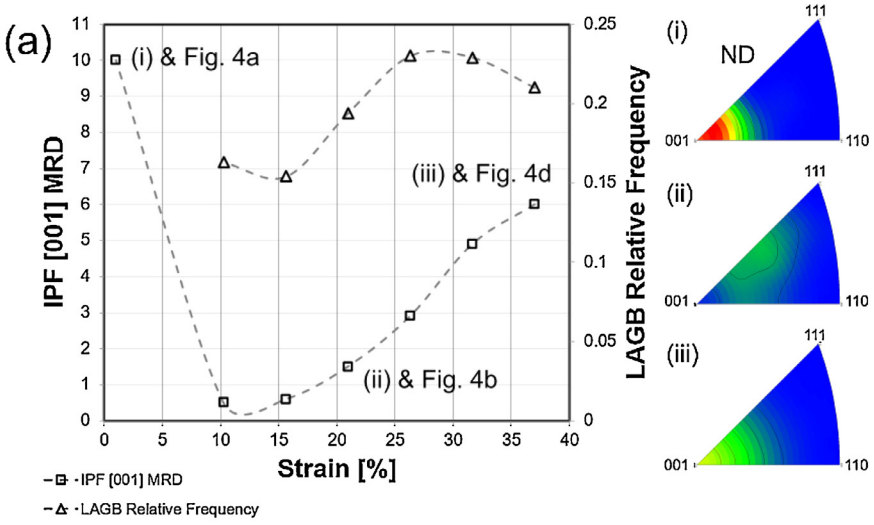

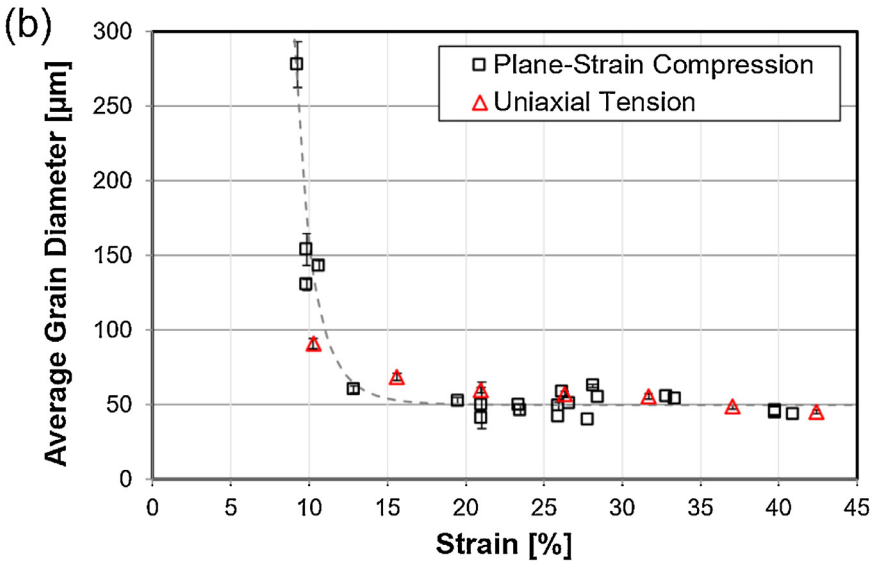

Fig. 5. Statistical EBSD data from along the sample gauge length of the rapidly heat treated sample shown in Fig. 4, as a function of the local strain showing; (a) strength of the <001>$_\beta$ // ND pole in MRD and the relative frequency of LAGBs (compared to HAGBs), (b) the average recrystallized β-grain sizes compared to previous results for the plane strain compression study conducted in ref. [12]. In (a) the IPFs (i-iii) correspond to the pole figures in Fig. 4a,b,d, respectively, and show the texture change with position.

strain measured from the sample's reduction in area. This data shows close agreement with the original PSC results, and confirms the same dramatic onset of grain refinement by rapid recrystallization at a low strain level of ~ 9%, although with the new tensile sample results, there is a slightly greater reduction in grain size with increasing strain in the range from where recrystallization becomes active, to the high strain region near the fracture surface. The flatter plateau seen in the original PSC tests was probably caused by the greater heterogeneity of the strain distribution in the test geometry, which was underestimated by the FE analysis used to account for the effects of friction in the PSC tests. However, it remains to be addressed why a nearly constant grain size is seen with increasing strain level once the threshold is reached to initiate recrystallization. As the whole sample was heat treated uniformly, this may be because of the competition between the two mechanisms involved, which is controlled by the relative density of their respective recrystallization nuclei. Rapid grain growth also occurs in Ti64 above its β transus temperature [12,32] which, owing to the pseudo-parabolic response, will tend to equilibrate differences in the grain size caused by a difference in nucleation density.

4 Conclusions

This work was conducted to attempt to clarify a previous observation [20] that a unique recrystallization mechanism may be occurring in lightly deformed, fine-scale Ti64 lamellar transformation microstructures, when subject to rapid heating rates, as are typical in an AM process. This mechanism was first hypothesised after an unusual micro-texture was observed in a deformed and rapidly re-heated parent β grain [12,20], that could not be related to the deformation texture, and the realisation it could be reproduced from the parent grain orientation by the {112}<111> β twinning system. It was also noted in our previous plane strain compression simulations, that this mechanism was probably operating in competition with conventional recrystallization, which involved local lattice rotation within intense shear bands that were caused by the die-sample friction conditions in plane strain compression tests. Therefore, by using an entirely different tensile deformation mode, it was hoped that more independent evidence could be found for this interesting possibility.

The new experimental evidence further supports the β twinning argument. Analysis of the strained and rapidly heated samples has again revealed a highly refined recrystallized β microstructure, after low strain deformation, which exhibited a four-fold symmetric texture motif centred around their parent {001}$_\beta$ // ND grain orientations, which was similar to that seen in the PSC experiments, despite the use of an entirely different deformation mode. The new texture also again completely consumed the original {001}$_\beta$ // ND solidification texture. Furthermore, the micro-texture seen at lower deformation strains was replaced by a more conventional recrystallization texture as the strain level increased closer to the fracture surface, where greater matrix lattice rotation would be expected.

Declaration of Competing Interest

The authors declare that they have no known competing financial interests or personal relationships that could have appeared to influence the work reported in this paper.

Acknowledgements

The authors are appreciative of the EPSRC grants (LightForm - EP/R001715/1; NEWAM – EP/R027218/1) and Innovate UK (Open Architecture Additive Manufacturing, OAAM) for supporting aspects of this research. P.B. Prangnell is also grateful to the Royal Academy of Engineering, UK, and Airbus for financial support through the Airbus-University of Manchester Centre for Metallurgical Excellence.

Supplementary materials

Supplementary material associated with this article can be found, in the online version, at doi:10.1016/j.mtla.2020.100857.

References

[1] S.W. Williams, F. Martina, A.C. Addison, J. Ding, G. Pardal, P.A. Colegrove, Wire + arc additive manufacturing, Mater. Sci. Technol. 32 (7) (2016) 641–647, doi:10.1179/1743284715Y.0000000073.
[2] T. Duda, L.V. Raghavan, 3D metal printing technology, IFAC-PapersOnLine 49 (29) (2016) 103–110, doi:10.1016/j.ifacol.2016.11.111.
[3] T. DebRoy, et al., Additive manufacturing of metallic components - process, structure and properties, Prog. Mater. Sci. 92 (2018) 112–224, doi:10.1016/j.pmatsci.2017.10.001.
[4] J. Allen, An investigation into the comparative costs of additive manufacture vs. machine from solid for aero engine parts, Proc. Meet. RTO-MP-AVT-139 (2006) 17-1-17–10, doi:10.14339/RTO-MP-AVT-139-17.
[5] F. Martina, J. Mehnen, S.W. Williams, P.A. Colegrove, F. Wang, Investigation of the benefits of plasma deposition for the additive layer manufacture of Ti-6Al-4V, J. Mater. Process. Technol. 212 (6) (2012) 1377–1386, doi:10.1016/j.jmatprotec.2012.02.002.
[6] F. Wang, S.W. Williams, P.A. Colegrove, A.A. Antonysamy, Microstructure and mechanical properties of wire and arc additive manufactured Ti-6Al-4V, Metall. Mater. Trans. A Phys. Metall. Mater. Sci. 44 (2) (2013) 968–977, doi:10.1007/s11661-012-1444-6.
[7] D. Ding, Z. Pan, D. Cuiuri, H. Li, Wire-feed additive manufacturing of metal components: technologies, developments and future interests, Int. J. Adv. Manuf. Technol. 81 (1–4) (2015) 465–481, doi:10.1007/s00170-015-7077-3.
[8] K.M. Taminger, R.A. Hafley, Electron beam freeform fabrication for cost effective near-net shape manufacturing, Spec. Meet. Cost Eff. Manuf. Net Shape Process. (NATO/RTO AVT-139) 16 (2006) 1–10.
[9] F. Martina, S.W. Williams, P.A. Colegrove, Improved microstructure and increased mechanical properties of additive manufacture produced Ti-6Al-4V by interpass cold rolling, SFF Symp. (2013) 490–496, doi:10.1007/s13398-014-0173-7.2.
[10] J. Donoghue, A.A. Antonysamy, F. Martina, P.A. Colegrove, S.W. Williams, P.B. Prangnell, The effectiveness of combining rolling deformation with Wire-Arc Additive manufacture on β-grain refinement and texture modification in Ti-6Al-4V, Mater. Charact. 114 (2016) 103–114, doi:10.1016/j.matchar.2016.02.001.
[11] A. Ho, H. Zhao, J.W. Fellowes, F. Martina, A.E. Davis, P.B. Prangnell, On the origin of microstructural banding in Ti-6Al4V wire-arc based high deposition rate additive manufacturing, Acta Mater. 166 (2019), doi:10.1016/j.actamat.2018.12.038.
[12] A.E. Davis, J.R. Kennedy, J. Ding, P.B. Prangnell, The effect of processing parameters on rapid-heating β recrystallization in inter-pass deformed Ti-6Al-4V wire-arc additive manufacturing, Mater. Charact. 163 (February) (2020), doi:10.1016/j.matchar.2020.110298.
[13] J. Gockel, J. Beuth, K.M. Taminger, Integrated control of solidification microstructure and melt pool dimensions in electron beam wire feed additive manufacturing of ti-6al-4v, Addit. Manuf. 1 (2014) 119–126, doi:10.1016/j.addma.2014.09.004.
[14] M.J. Bermingham, D.H. StJohn, J. Krynen, S. Tedman-Jones, M.S. Dargusch, Promoting the columnar to equiaxed transition and grain refinement of titanium alloys during additive manufacturing, Acta Mater. 168 (2019) 261–274, doi:10.1016/j.actamat.2019.02.020.
[15] A.A. Antonysamy, J. Meyer, P.B. Prangnell, Effect of build geometry on the β-grain structure and texture in additive manufacture of Ti6Al4V by selective electron beam melting, Mater. Charact. 84 (2013) 153–168, doi:10.1016/j.matchar.2013.07.012.
[16] M.J. Bermingham, S.D. McDonald, M.S. Dargusch, D.H. St.John, Grain-refinement mechanisms in titanium alloys, J. Mater. Res. 23 (1) (2008) 97–104, doi:10.1557/jmr.2008.0002.
[17] M.J. Bermingham, S.D. McDonald, D.H. StJohn, M.S. Dargusch, Segregation and grain refinement in cast titanium alloys, J. Mater. Res. 24 (4) (2009) 1529–1535, doi:10.1557/jmr.2009.0173.
[18] J.A. Koepf, M.R. Gotterbarm, M. Markl, C. Körner, 3D multi-layer grain structure simulation of powder bed fusion additive manufacturing, Acta Mater. 152 (2018) 119–126, doi:10.1016/j.actamat.2018.04.030.
[19] X. Bai, et al., Numerical analysis of heat transfer and fluid flow in multilayer deposition of PAW-based wire and arc additive manufacturing, Int. J. Heat Mass Transf. 124 (2018) 504–516, doi:10.1016/j.ijheatmasstransfer.2018.03.085.
[20] J. Donoghue, et al., On the observation of annealing twins during simulating β-grain refinement in Ti-6Al-4V high deposition rate AM with in-process deformation, Acta Mater. 186 (2019) 229–241, doi:10.1016/j.actamat.2020.01.009.
[21] F.J. Humphreys, M. Hatherly, Recrystallization and Related Annealing Phenomena, Elsevier, Oxford, 1996.
[22] D. Lunt, et al., Microscopic strain localisation in WAAM Ti-6Al-4V during uniaxial tensile loading, in: Proc. 13th World Conf. Titan., 2019.
[23] D. Lunt, et al., The effect of loading direction on strain localisation in wire arc additively manufactured Ti-6Al-4V, Mater. Sci. Eng. A 788 (2020), doi:10.1016/j.msea.2020.139608.
[24] W. Roberts, J. Gong, A.J. Wilkinson, E. Tarleton, Tension–compression asymmetry of <;c+a> slip in Ti-6Al, Scr. Mater. 178 (2020) 119–123, doi:10.1016/j.scriptamat.2019.11.002.
[25] J. Zhao, L. Lv, K. Wang, G. Liu, Effects of strain state and slip mode on the texture evolution of a near-α TA15 titanium alloy during hot deformation based on crystal plasticity method, J. Mater. Sci. Technol. 38 (2020) 125–134, doi:10.1016/j.jmst.2019.07.051.
[26] P.S. Davies, B.P. Wynne, W.M. Rainforth, M.J. Thomas, P.L. Threadgill, Development of microstructure and crystallographic texture during stationary shoulder friction stir welding of Ti-6Al-4V, Metall. Mater. Trans. A Phys. Metall. Mater. Sci. 42 (8) (2011) 2278–2289, doi:10.1007/s11661-011-0606-2.
[27] P.S. Davies, An Investigation of Microstructure and Texture Evolution in the Near-α Titanium Alloy Timetal 834, University of Sheffield, 2009.
[28] N. Gey, M. Humbert, Specific analysis of EBSD data to study the texture inheritance due to the $\beta \rightarrow \alpha$ phase transformation, J. Mater. Sci. 38 (6) (2003) 1289–1294, doi:10.1023/A:1022842712172.
[29] M. Humbert, N. Gey, The calculation of a parent grain orientation from inherited variants for approximate (b.c.c.-h.c.p.) orientation relations, J. Appl. Crystallogr. 35 (4) (2002) 401–405, doi:10.1107/S0021889802005824.
[30] J.R. Hönnige, et al., The effectiveness of grain refinement by machine hammer peening in high deposition rate wire-arc AM Ti-6Al-4V, Metall. Mater. Trans. A (2020).
[31] R.K. Sabat, M.V.S.S.D.S. Surya Pavan, D.S. Aakash, M. Kumar, S.K. Sahoo, Mechanism of texture and microstructure evolution during warm rolling of Ti-6Al-4V alloy, Philos. Mag. 98 (28) (2018) 2562–2581, doi:10.1080/14786435.2018.1493237.
[32] S.L. Semiatin, J.C. Soper, I.M. Sukonnik, Short-time beta grain growth conventional kinetics alloy, Acta Metall. 44 (5) (1996) 1979–1986, doi:10.1016/1359-6454(95)00311-8.